LAWRENCE
LIVERMORE
NATIONAL
LABORATORY

LLNL-JRNL-763450

Negative differential conductivity in liquid aluminum from real-time quantum simulations

X. Andrade, S. Hamel, A. A. Correa

December 3, 2018

European Journal of Physics B

Disclaimer

This document was prepared as an account of work sponsored by an agency of the United States government. Neither the United States government nor Lawrence Livermore National Security, LLC, nor any of their employees makes any warranty, expressed or implied, or assumes any legal liability or responsibility for the accuracy, completeness, or usefulness of any information, apparatus, product, or process disclosed, or represents that its use would not infringe privately owned rights. Reference herein to any specific commercial product, process, or service by trade name, trademark, manufacturer, or otherwise does not necessarily constitute or imply its endorsement, recommendation, or favoring by the United States government or Lawrence Livermore National Security, LLC. The views and opinions of authors expressed herein do not necessarily state or reflect those of the United States government or Lawrence Livermore National Security, LLC, and shall not be used for advertising or product endorsement purposes.

LAWRENCE
LIVERMORE
NATIONAL
LABORATORY

LLNL-JRNL-763450

Negative differential conductivity in liquid aluminum from real-time quantum simulations

X. Andrade, S. Hamel, A. A. Correa

December 3, 2018

European Journal of Physics B

Disclaimer

This document was prepared as an account of work sponsored by an agency of the United States government. Neither the United States government nor Lawrence Livermore National Security, LLC, nor any of their employees makes any warranty, expressed or implied, or assumes any legal liability or responsibility for the accuracy, completeness, or usefulness of any information, apparatus, product, or process disclosed, or represents that its use would not infringe privately owned rights. Reference herein to any specific commercial product, process, or service by trade name, trademark, manufacturer, or otherwise does not necessarily constitute or imply its endorsement, recommendation, or favoring by the United States government or Lawrence Livermore National Security, LLC. The views and opinions of authors expressed herein do not necessarily state or reflect those of the United States government or Lawrence Livermore National Security, LLC, and shall not be used for advertising or product endorsement purposes.

LLNL-JRNL-763450

Negative differential conductivity in liquid aluminum from real-time quantum simulations

Xavier Andrade, Sébastien Hamel, and Alfredo A. Correa
Lawrence Livermore National Laboratory, 7000 East Avenue, Livermore, CA 94550, USA

The conduction of electricity in materials is usually described by Ohm's law, which is a first order approximation to a more complex and non-linear behavior. It is well known that in some semiconductors, the conductivity, the constant that relates voltage and current, changes for high enough currents. In this work we predict for the first time that a metal, liquid aluminum, exhibits negative-differential conductivity, a non-linear effect where the current decreases as the applied voltage is increased. We observe this change in the conductivity for very high current densities of the order of $10^{12} - 10^{13}$ A/cm^2. Our predictions are based on a computational approach that can atomistically model, for the first time, non-linear effects in the conductivity from first principles by following in real-time the quantum dynamics of the electrons. From our simulations, we find that the change in the non-linear conductivity emerges from a competition between the current-induced accumulation of charge around the nuclei, which increases the scattering of the conduction electrons, and a decreasing ion-scattering cross-section at high currents. Our results illustrate how normal matter behaves under extreme fields that will become available from free electron lasers and other future experiments.

I. INTRODUCTION

In 1827, Georg Ohm discovered that when a voltage is applied over a piece of a certain material, it will carry a current proportional to that voltage. The proportionality constant depends on the geometry of the conductor, and an intrinsic property of the material, the conductivity. Since then, the conductivity has become one of the basic quantities that characterize a material.

Ohm's law is, in fact, a first order approximation to a more complex behavior: many materials, diodes for example, do not follow Ohm's law. Even for those that do, we can expect that for large enough voltages the conductivity will change. In some materials the current decreases as the voltage is increased, leading to the phenomenon of negative differential conductivity (also known as negative differential resistance) [1–3]. Negative differential conductivity has been observed in semiconductors, like GaAs or GaN, where it is used for technological applications [4, 5]. It has also been reported in molecular electronic devices [6–9] and nano-structures [10–16]. As experimental facilities become capable of delivering electric fields close to the atomic fields the electrons feel in an atom [17, 18], even normal metals could potentially exhibit anomalous electrical properties under these conditions. However, little is known on how matter behaves under these extreme fields, because most theories and experiments only probe the linear response to external fields.

In this work we study the non-linear conductivity of pure liquid aluminum, and predict that it presents negative differential conductivity. As far as we know, this is the first time this phenomenon has been reported in a bulk metal. Our simulations indicate that the currents needed to observe this effect are in excess of 10^{12} A/cm^2, larger than what is currently possible in experiments.

The non-linear behavior at those large currents appears when the associated drift velocity is close to the Fermi velocity of the conduction electron in the material. In this regime, our computational simulations show that the electron scattering increases due to the accumulation of electron density around atoms, lowering the effective conductivity. For even higher currents, the effective conductivity increases rapidly due to the ballistic reduction of the scattering cross section. To interpret the results of our simulations, we develop a model for the conductivity by recasting the problem into one of fast ions moving in an electron gas. This simple model captures the main aspects of the non-linear conduction.

Our breakthrough prediction is made possible by a new method to simulate conduction of electric current in metals based on real-time dynamics. We directly simulate the process of electrons moving across the material; we apply an external electric field, and we follow the response of the material by following the quantum dynamics of the electrons in real-time. By controlling the intensity of the applied field, we gain access to the non-linear regime that was until now out of reach to computational methods.

From a first-principles perspective, the electrical conductivity of condensed matter is usually calculated using perturbation theory, by combining density-functional theory (DFT) and the Kubo-Greenwood formula [19, 20]. This method only yields the conductivity in the low current regime, so it is not suitable to predict non-linear effects in the conductivity.

It would be tempting to calculate non-linear conductivity by getting higher order response coefficients. However, it is generally accepted that a systematic power expansion of the transport coefficients, of which the Kubo-Greenwood/Green-Kubo is the first term, is not reliable to obtain non-linear effects, as these coefficients are non-analytic functions of the driving thermodynamic forces, the voltage difference in this case [21]. This is the reason for using a method like real-time electron dynamics

that can directly model the response to strong fields to all orders.

II. THEORY

We start by briefly introducing our simulation approach. We base our calculations on time-dependent density functional theory (TDDFT) [22], as its computational cost allows us to simulate systems with enough atoms to capture the effect of disorder, which is crucial to describe conduction accurately. The method is applicable for any theoretical framework that can model the dynamics of the electrons in a material.

The conductivity is defined by Ohm's law [23, 24] $\mathbf{J}(\omega) = \sigma(\omega)\,\mathbf{E}(\omega)$, which relates a monochromatic external electric field, at a frequency ω, and the current density it generates. In a real-time simulation, instead of a frequency-resolved perturbation, we apply a time-resolved field $\mathbf{E}(t)$ and then follow the current density evolution $\mathbf{J}(t)$. While we can select any temporal dependency for the electric field, it is convenient to perturb the system using a *kick* [25]: a field of the form $\mathbf{E}(t) = \mathbf{E}_0\delta(t)$, where $\mathbf{E}_0$ determines the intensity and direction of the field. By inserting this kick into Ohm's law, the conductivity can be calculated from the time-dependent current density obtained from the simulation as [26]

$$\sigma(\omega) = \frac{1}{E_0}\int_0^\infty \mathrm{d}t\, \mathrm{e}^{-\mathrm{i}\omega t} J(t)\ . \tag{1}$$

There are several advantages in applying the external perturbation as a *kick*. First, this external pertubation containts all the frequencies with the same intensity and the response at individual frequencies can be obtained by a Fourier analysis. Second, conductivity must be expressed to the response to *external* fields, as opposed to *induced* fields. This way of perturbing the system naturally separates the external and the induced field in the time domain. The external macroscopic (controlled) field only exists at $t = 0$, while at $t > 0$ all fields (macroscopic and microscopic) are induced.

A key aspect of our simulation is the ability to include an electric field $\mathbf{E}$ of finite intensity, in order to induce a current in the system. Usually, the electric field enters into the TDDFT equations through an external scalar potential; however, the scalar potential associated to a uniform electric field does not satisfy the periodic boundary conditions used to describe an extended system. Instead, we use a gauge where the uniform electric field is generated by a uniform, but time-dependent, vector potential $\mathbf{A}$ as [27] (Gaussian atomic units are used throughout)

$$\mathbf{E}(t) = -\frac{1}{c}\frac{\partial \mathbf{A}(t)}{\partial t}\ . \tag{2}$$

The fundamental *observable* in our approach is the time-dependent macroscopic current density $\mathbf{J}$, which in TDDFT can be readily calculated from the time-evolving orbitals of Kohn-Sham formalism. However, care must be taken into making the current properly gauge invariant, by including the diamagnetic contribution and the additional terms [27] that come from non-local pseudopotentials [28] that represent the ions.

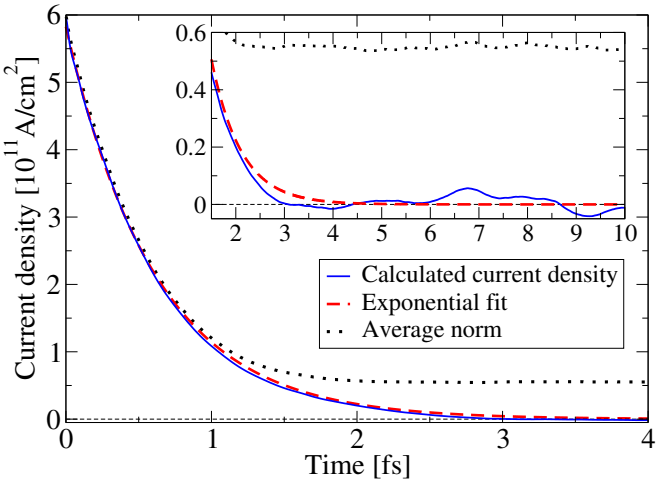

Figure 1. Current density *vs.* time after a kick of 0.1 a.u. (continuous blue line) for a specific ionic configuration of a supercell with 256 aluminum atoms in the liquid phase. The inset shows in detail the current fluctuations around zero for long times. The red segment line shows an exponential fit to the current, based on the range $0 < t < 0.5$ fs. The dotted black line shows the spatial average of the absolute value of the local current density, which illustrates how the macroscopic current density decays due to a randomization of the microscopic local current density, which retains a finite intensity.

III. RESULTS

For our study, we consider liquid aluminum, as a prototypical metal, at high temperature (0.5 eV $\sim$ 5802 K) and near solid density (2.7 g/cm^3). The liquid state is chosen to simplify the problem as in this state, the intrinsic disorder avoids pathologies that can arise in a crystalline system and its associated translation symmetries. In a perfect crystalline solid, an initial current would produce Bloch waves that support persistent (non-decaying) currents.[30]

Our simulation supercell contains 256 atoms and we use the gamma point for Brillouin zone sampling. The TDDFT scheme is implemented in the real-space code Octopus [31, 32]. For the real-time TDDFT simulations in this article we use the adiabatic local density approximation (ALDA), a grid spacing of 0.425 a.u., and an electronic time step of 0.1 a.u. = 0.00242 fs.

We start by showing the results for a single simulation using one snapshot of a molecular dynamics (MD) run. In Fig. 1 we plot the current density evolving in time

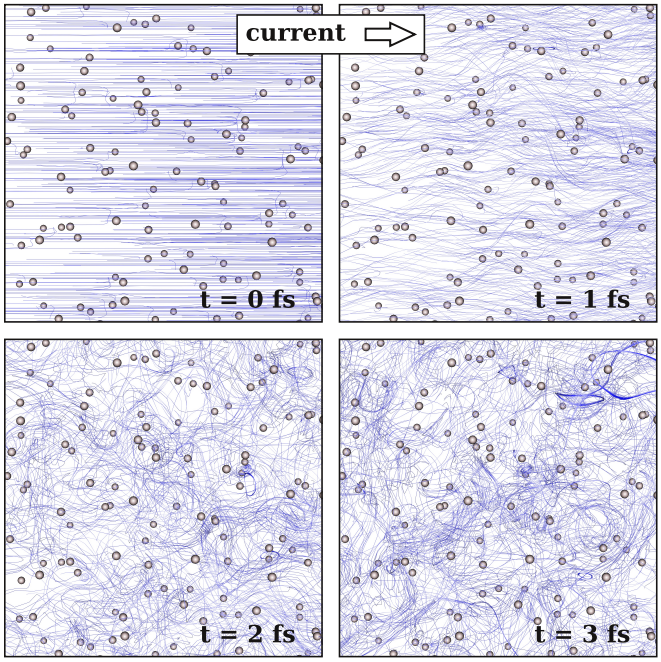

Figure 2. Stream lines of the microscopic current density for different times for a kick of 0.1 a.u. in liquid aluminum. Initially the lines are parallel and follow the direction of the current (from left to right), as time passes the current density becomes more disordered and isotropic. This disorder in the direction of the local current density is partially responsible for making the average current density vanish. The stream lines represent the trajectories of fictitious particles under the microscopic current density as a velocity field. They are generated by the VisIt program [29].

after a kick of 0.1 a.u. ($\sim 2.1 \times 10^{27}$ V/ms). As seen in the figure, the current steadily decays towards zero. Still, small fluctuations of the current are observed after it has decayed (as seen on the inset of Fig. 1). Through a function fit (for $t < 0.5$ fs) we can see that the current decay is very close to exponential.

The real-time simulation allows us to get insight into the nature of the decay process. Since the macroscopic current density is the spatial average of the microscopic current density, the current density might decay because the microscopic local current density is decaying to zero at each point, which is to be expected of a final time-reversible quantum state. Alternatively, it is possible that the local current density becomes disordered, making the average zero while retaining a finite value at each point.

To differentiate between those two scenarios we consider the microscopic current density of the system. In Fig. 1 we include the average value of the norm of the microscopic current density, and in Fig. 2 we plot the streamlines of the current density for different times.

Initially, both the current density and its average norm decay in a similar fashion. However, after some time the average norm remains constant while the average current continues decaying. This tells us that both decay mechanisms are at play: initially ($t < 1$ fs) there is a local decay of the *magnitude* of the current, but later ($t > 1$ fs) the *directional disorder* and spatial randomness of the current are responsible for nullifying the average current. Interestingly, these results show a fundamentally irreversible process in the simulation of a quantum system of many electrons from microscopically reversible equations.

Therefore, we find several effects. First, the average current density (which we identify with the macroscopic current) decays to zero. This behavior is not surprising and it is compatible with the concept of resistivity by ion scattering, in which the macroscopic current eventually ceases if no new external field is applied. Second, we also note that for this finite system there is a residual fluctuating current. Third, there are persistent microscopic local currents that fluctuate spatially and temporally.

These last two effects are not obvious and require some discussion, as one may expect that for long times all the currents, macroscopic and microscopic, would cease. To find an explanation, we have to take into account that this simulated system is closed, and the energy is conserved. As such, the electronic system can never reach a ground state, or any eigenstate of the many-body quantum system for that matter. Instead, we find that the system dynamics reaches a macroscopic steady state by a rich, persistently evolving microscopic state. This is analogous to the result we would expect from a classical simulation of particles under molecular dynamics of a closed system. There is no principle that will prevent the electrons to keep dynamically evolving at long times, given that there is no energy sink applied to our system of electrons; yet we find the expected relaxation in a macroscopic description. We believe that this is not an artifact of the approximations utilized for TDDFT, and that in spite of the approximations of TDDFT the overall mechanism is correct.

To obtain the frequency-dependent conductivity we Fourier-transform the time-dependent current density, according to Eq. 1. We can do a numerical Fourier transform of the current, or analytically transform the exponential fit, which gives us a Drude-like form for the conductivity. Both results are shown in Fig. 3, where we compare them with the results from Kubo-Greenwood [19, 20] for the same snapshot of the ionic configuration. It can be observed that there is a good agreement between real-time TDDFT and Kubo-Greenwood, where the conductivity is a sum over discrete transitions between orbitals, so a broadening of 0.03 eV is applied to produce a continuous curve. Still, the conductivity is rougher than the real-time approach. The small differences in the results can be attributed to the additional approximations introduced in Kubo-Greenwood: the truncation of the sum over unoccupied states, and the lack of a full self-consistent response. The approximate agreement with Kubo-Greenwood in the linear regime validates the method.

The results we have shown so far correspond to a single

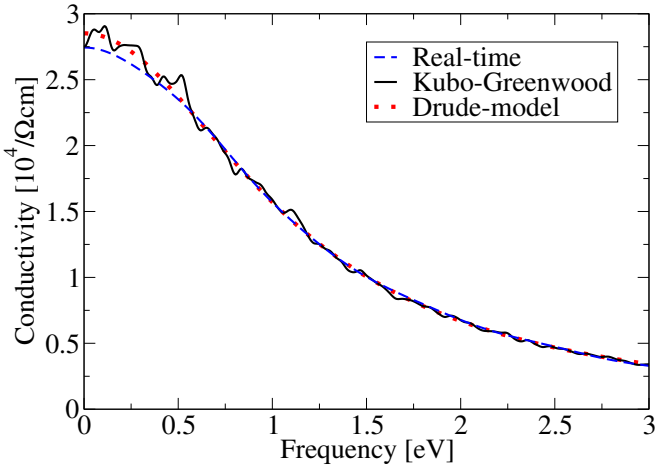

Figure 3. Frequency-dependent conductivity in the low frequency regime (blue segmented line), calculated as a Fourier transform of the time-dependent current density (Eq. 1). We compare it with the frequency-dependent conductivity calculated by the Kubo-Greenwood method (black continuous line), for the same ionic snapshot. 3000 bands are used, which allows for vertical excitation energies of up to 40 eV. Additionally, a Drude fit, obtained from the Fourier transform of the exponential fit of the real time current, is presented for comparison (red dotted line). These results are for a single ion configuration (snapshot) for a fair comparison between the two methods.

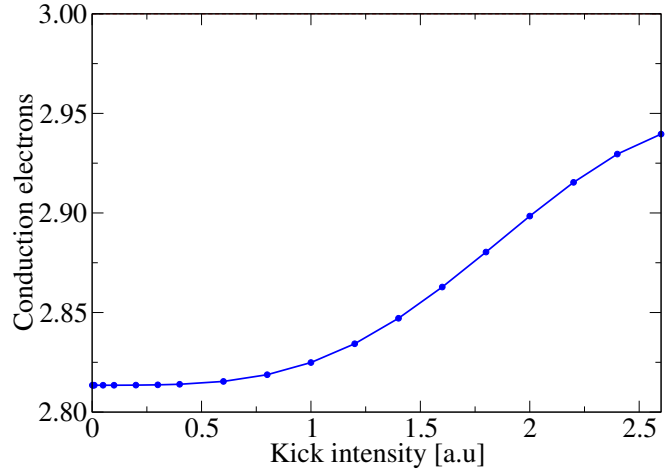

Figure 4. Ratio of the initial current per atom with respect to the applied kick. This number is equivalent to the fraction of the electrons per atom that participate in the current near time zero. The value grows as the intensity of the kick increases and approaches 3, coinciding with the valence electrons in aluminum.

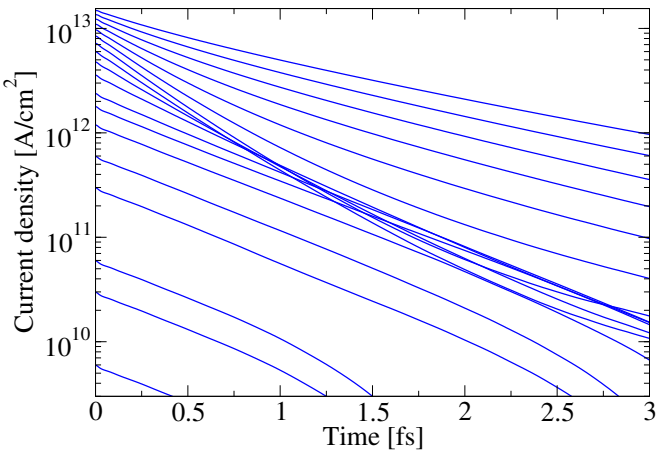

Figure 5. Time-evolution of the current density for a family of initial conditions with different intensities of electric *kick*, and therefore initial current densities, averaged over ionic configurations. For initial current below 10^{12} A/cm^2 we observe a decay with the same time constant, as expected from a linear response. For larger perturbations we enter into a non-linear regime that is evidenced by the changing slopes of the graphs.

snapshot, which serves to illustrate the detailed properties of our simulations. However, if we want to make predictions, we need to average the results over multiple ionic configurations obtained from MD. We took 200 ionic snapshots from a 12 ps equilibrated MD run at 5802 K using VASP [33] at the LDA level of approximation to the exchange-correlation functional, and a 2x2x2 Monkhorst-Pack grid (MD time step of 2 fs). For each snapshot we calculated the evolution of the current for different kick intensities, from 0.001 to 2.6 a.u., which allows us to access linear and non-linear effects. As before, the only role of MD is to generate snapshots.

We first check how the initial current depends on the kick by calculating the ratio of the initial current density over the kick intensity, which we plot in Fig. 4. Since the current corresponds to the momentum of the electrons, it can be shown that this ratio is essentially the amount of charge that participates in the conduction. In a disordered metallic system this value, when normalized per atom, should be close to the valence charge. We see that for small kicks below 0.5 a.u., a constant fraction of around 2.81 electrons per atom are excited, while for higher intensity kicks this value starts to grow and saturates towards 3 for the kicks considered, which coincides with the valence charge for aluminum.

We now consider the decay behavior to determine the linearity of the response with respect to the intensity of the perturbation. For each kick intensity we obtain the current density, averaged over configurations, as a function of time. The values are shown, in logarithmic scale, in Fig. 5. If we consider that the slope of the current decay gives us an idea of the value of the conductivity, we can clearly see that there is a non-linear behavior.

For each curve of Fig. 5, we determine the zero-frequency conductivity by an exponential fit to the initial part of the time-dependent current ($t < 0.5$ fs) that we insert into Eq. 1. The resulting conductivity *vs.* initial current is shown in Fig. 6. The figure shows that the

conductivity exhibits a clear dependency with the current density. For low currents, we obtain a conductivity of 3.0×10^4 $(\Omega\,\mathrm{cm})^{-1}$ that is close to the $\omega \to 0$ extrapolated Kubo-Greenwood value of 2.8×10^4 $(\Omega\,\mathrm{cm})^{-1}$, which we calculated from the same set of snapshots (Fig. 3). These values are also consistent with previous theoretical results [34–38]. For higher intensities, the conductivity is not constant and exhibits a minimum value of $\sim 1.7 \times 10^4$ $(\Omega\,\mathrm{cm})^{-1}$ for $\sim 7.2 \times 10^{12}$ A/cm^2 which corresponds to a kick, or electronic velocity, of ~ 1.2 a.u., comparable to the effective Fermi velocity for this system: 0.92 a.u.. For larger currents the conductivity increases rapidly.

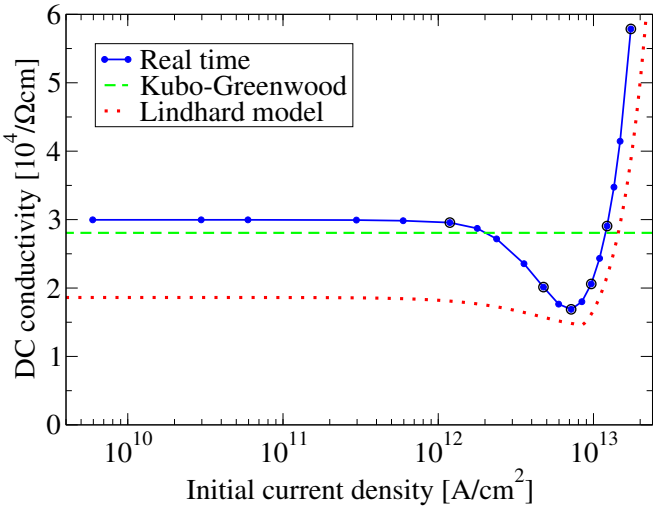

Figure 6. Zero-frequency conductivity as a function of the current density. For low currents the value of the conductivity agrees with Kubo-Greenwood, and at large currents there is a minimum of conductivity at $\sim 7 \times 10^{12}$ A/cm^2. At even larger currents the conductivity increases as the electrons become less affected by scattering processes. The points encased in a black circle indicate the values of the current in the cases shown in Fig. 7. Dotter red curve is the result of a simple model 3 built to understand the origin of the minimum of conductivity.

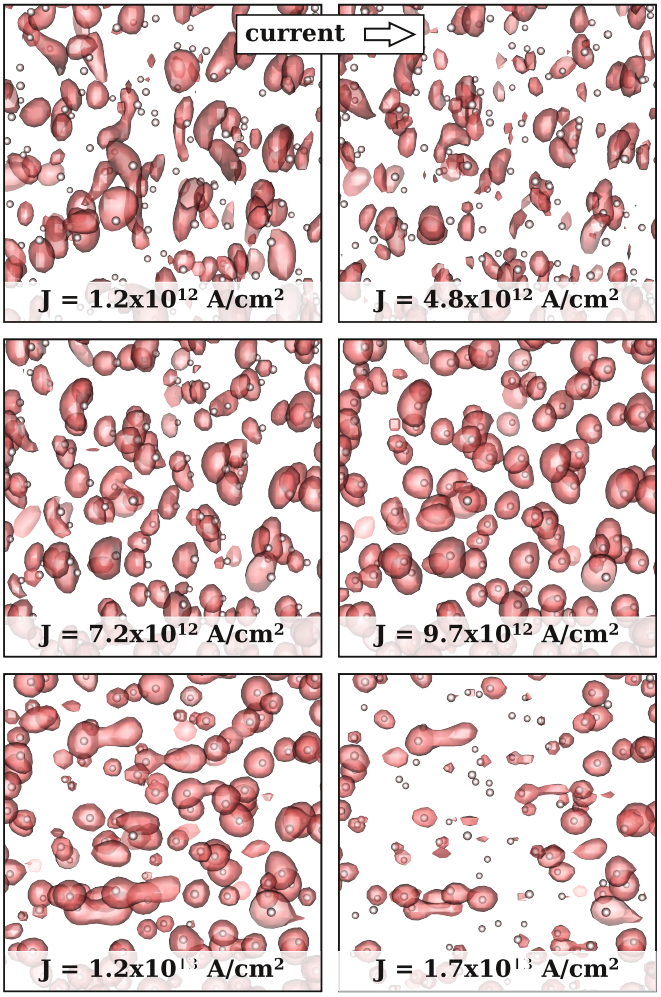

Figure 7. Regions of accumulation of electronic charge for different values of the initial current, for a single snapshot. The red surfaces represent isosurfaces of the difference of the density at time 0.242 fs with respect to the ground state density. The corresponding values of the conductivity for each current are shown encased in a black circle in Fig. 6. The values of the isosurfaces are proportional to the perturbation intensity and are 0.0025, 0.01, 0.015, 0.02, 0.025 and 0.03 a.u., respectively.

To elucidate the origin of the non-linearity in the conductivity, we plot in Fig. 7 the change in the electronic density for different initial currents for a particular snapshot and a fixed time. It can be seen that there is a clear change in regime depending on the initial currents. For low currents there is some small accumulation of charge, mainly in the interatomic regions. For larger currents the charge starts to accumulate close to the nuclei. For $\sim 7.2 \times 10^{12}$ A/cm^2, which is close to the conductivity minimum, the accumulation of the charge occurs in front of the atoms. As the current is increased, the charge accumulation regions are centered around the atoms, and appendices form behind some of the atoms. Finally, for large currents these regions of charge accumulation start to disappear, matching the rapid increase in conductivity.

We theorize that the generation of these regions of charge accumulation increase the amount of scattering that the electrons are subject to, reducing the conductivity. At the same time, for larger currents we expect the conductivity to increase, as the electrons become ballistic and are less affected by scattering processes. The combination of these two effects explain the shape of the conductivity curve that we see in Fig. 6.

The theory used for the simulations, TDDFT in the ALDA approximation, constitutes the simplest form of the KS equations, where electrons interact through a mean field potential and dynamical many-body effects are neglected. Other many-body theories of TDDFT [39] and classical corrections [40] have been proposed, at ad-

ditional computational cost, as corrections for the linear residual resistivity of metals and non-degenerate plasmas. However, the explanation based on charge accumulation for the minimum of the conductivity would hold even in the presence of many-body effects.

In order to further understand our results and show that this is a physical pheonomenon, in this section we provide a simple semi-analytic formulation of the problem of non-linear conductivity based on the high-energy Lindhard ion-in-jellium scattering theory [41] that we compare with our first principles results.

The formula we propose is derived from electronic stopping power theory [42], where the collective force on the ions is reinterpreted, by a change of the frame of reference, as a deacceleration of the electronic stream. In this interpretation, we have an electronic stopping power problem of several ions moving with effective charge Z through an electron gas with a certain effective valence electron density.

In the linear-response theory of Lindhard (linear in Z), the approximated *drag* force on the moving ion is a double integral in the wavenumber and frequency of the electron energy loss function associated with the dielectric function.

$$F^{\mathrm{drag}} = 2Z^2 \frac{e^2}{\pi v^2} \int_0^\infty \frac{\mathrm{d}k}{k} \int_0^{kv} \mathrm{d}\omega\, \omega\, \mathrm{Im}\left(\frac{-1}{\varepsilon(k,\omega)}\right)$$

In the frame of reference of the electrons, the total drag force on the ions is exactly opposite to the force applied to the electrons that constitute the electric current. Taking into account that there are Z free electrons per ion and that a current J has an associated drift velocity $v = J/n$, the electrical conductivity due to scattering results to be approximated by

$$\sigma(J) = \frac{\pi}{2}\frac{J^2}{Zn}\left(\int_{1/R_\mathrm{s}}^\infty \frac{\mathrm{d}k}{k} \int_0^{kJ/n} \mathrm{d}\omega\, \omega\, \mathrm{Im}\left[\frac{-1}{\varepsilon(\omega,k)}\right]\right)^{-1} \tag{3}$$

where Z is the number of valence participating electrons per ion, $\varepsilon(\omega, k)$ is some appropriate model of the dielectric response and n is the valence density. In the model, Z is assumed to be 3, based on the valence electrons in aluminum. R_s is an adjustable spatial cutoff introduced to capture a finite radius of action for each individual scatterer. The main effect of adjusting R_s is to control the vertical scale of the model curve. In our results, R_s is set to one fourth of the average interatomic distance, so that the model prediction adjusts to the high current portion of the results.

The model is formally justified at large currents as it is perturbative in Z/J; however as we can see from Fig. 6, it replicates qualitatively well the shape of the simulated conductivity, reproducing the main features of the curve: a constant value for low currents, a minimum close to the current corresponding to the Fermi velocity, and a conductivity that increases rapidly for large values. This divergence behaves as $\sim J^2/\log J$, as one would expect from the Born [43] and Coulomb-logarithm scattering theory [44]. The charge accumulation found here is analogous, in the problem of electronic stopping power, to the electronic trailing wakes produced by fast moving ions [45].

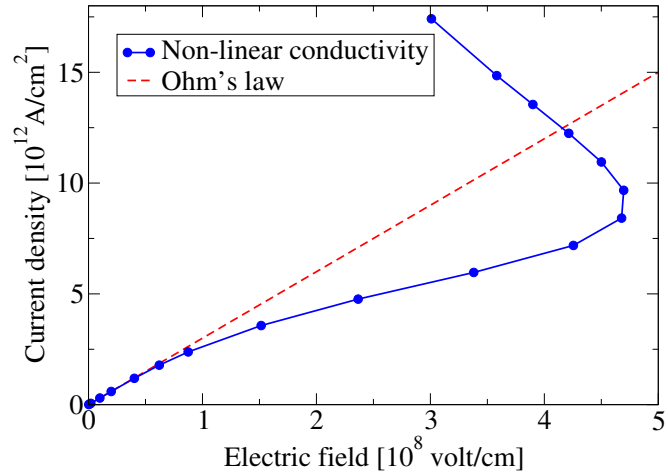

Figure 8. Current density *vs.* electric field curve for liquid aluminum calculated from the current dependency of the conductivity. It represent the relation $E = \sigma(J)J$ where the independent variable is J. This curve predicts that aluminum is an S-shape negative-differential conductor[1] for very high currents and fields.

Based on the conductivity results for each current density, we can obtain the electric field *vs.* current density curve shown in Fig. 8. It shows that our simulations predict a negative differential conductivity in liquid aluminum at 5800 K for electric fields of the order of 10^8 V/cm. The induced current density in this regime is of the order of $10^{12} - 10^{13}$ A/cm^2. We have not found an indication that this predicted effect has been directly measured before, as such regimes do not seem to be experimentally reachable today. The negative differential conductivity that we find is of S-type, or current-controlled [1]. In practice, a multi-valued current density for a given field, as we see in the figure, would cause the system to separate in different spatial domains with different conductivities [2]. We expect the curve to swing again to the right for higher currents, as semi-core electrons become involved in the conduction, recovering positive differential conductivity and completing the S shape.

IV. CONCLUSIONS

In conclusion, based on a new method to calculate the non-linear conductivity of bulk metals, we have studied the conductivity of liquid aluminum for very-high current densities ($> 10^{10}$A/cm^2). We find that in our simulations the conductivity changes under these conditions, leading us to predict that eventually aluminum

presents negative differential conductivity. While these results are currently outside of the range of experiments, the extreme field necessary to observe this effect will be reachable by the next generation of free electron lasers (FEL) [17, 46, 47].

We find this effect by first principles simulations in aluminum as a prototypical material, but the simplified model shows that this is an ubiquitous effect, likely to be found when drift velocity current approaches the natural velocities of the degenerate electron gas. It is also possible that the effect becomes accessible, in other metallic systems also tractable by this first principles simulation method, under extreme conditions of temperature or pressure that change the conduction electron density and the Fermi velocity. For example, an analogous effect, the 'two-stream instability', is known to develop in *classical* plasmas [48]. In fact, our results allow us to predict the onset of the non-linearity from the Fermi velocity and the valence charge of the material.

Our real-time method is certainly not restricted to electrical conductivity in metals, which is one of the simplest applications of modeling currents in materials. This first application opens the path for studying other phenomena that up to now have been beyond the reach of atomistic quantum simulations. For example, an interesting extension of our approach would be to study electronic thermal conductivity and mixed electrical-thermal transport properties, so that we can simulate, understand and predict non-linear effects in heat transport, including negative-differential heat conduction [49–51]. In our framework, it will require the introduction of recent developments of the description of thermal properties in TDDFT [52–54]. Our ultimate goal is to build a general theoretical and computational tool that can combine different types of perturbations and observables into time-resolved simulations. By accessing combined responses and non-linear effects, this tool would give us an unprecedented capacity to study different phenomena that are of interest in condensed matter physics, material science, and plasma physics.

ACKNOWLEDGEMENTS

This work was performed under DOE Contract No. DE-AC52-07NA27344. This work was supported as part of the Energy Dissipation to Defect Evolution (EDDE), an Energy Frontier Research Center funded by the US Department of Energy, Office of Science, Basic Energy Sciences. Computing support for this work came from the LLNL Institutional Computing Grand Challenge program. LLNL IM release number LLNL-JRNL-715217.

[1] B. K. Ridley, Proc. Phys. Soc. **82**, 954 (1963).
[2] A. F. Volkov and S. M. Kogan, Sov. Phys. Usp. **11**, 881 (1969).
[3] B. R. Pamplin, Contemp. Phys. **11**, 1 (1970).
[4] J. Gunn, Solid State Commun. **1**, 88 (1963).
[5] V. Gružinskis, J. H. Zhao, P. Shiktorov, and E. Starikov, Mater. Sci. Forum **297-298**, 341 (1999).
[6] J. Chen, Science **286**, 1550 (1999).
[7] Y. Xue, S. Datta, S. Hong, R. Reifenberger, J. Henderson, and C. Kubiak, Phys. Rev. B **59**, R7852 (1999).
[8] H. Dalgleish and G. Kirczenow, Nano Lett. **6**, 1274 (2006).
[9] M. L. Perrin, R. Frisenda, M. Koole, J. S. Seldenthuis, J. A. C. Gil, H. Valkenier, J. C. Hummelen, N. Renaud, F. C. Grozema, J. M. Thijssen, D. Dulić, and H. S. J. van der Zant, Nat. Nanotechnol. **9**, 830 (2014).
[10] I.-W. Lyo and P. Avouris, Science **245**, 1369 (1989).
[11] M. Rinkiö, A. Johansson, V. Kotimäki, and P. Törmä, ACS Nano **4**, 3356 (2010).
[12] X. Zheng, W. Lu, T. A. Abtew, V. Meunier, and J. Bernholc, ACS Nano **4**, 7205 (2010).
[13] Y. Wu, D. B. Farmer, W. Zhu, S.-J. Han, C. D. Dimitrakopoulos, A. A. Bol, P. Avouris, and Y.-M. Lin, ACS Nano **6**, 2610 (2012).
[14] Y. Du, H. Pan, S. Wang, T. Wu, Y. P. Feng, J. Pan, and A. T. S. Wee, ACS Nano **6**, 2517 (2012).
[15] Y.-C. Lin, R. K. Ghosh, R. Addou, N. Lu, S. M. Eichfeld, H. Zhu, M.-Y. Li, X. Peng, M. J. Kim, L.-J. Li, R. M. Wallace, S. Datta, and J. A. Robinson, Nat. Commun. **6**, 7311 (2015).
[16] P. B. Vyas, C. Naquin, H. Edwards, M. Lee, W. G. Vandenberghe, and M. V. Fischetti, Journal of Applied Physics **121**, 044501 (2017).
[17] P. Ball, Nature **548**, 507 (2017).
[18] E. Cartlidge, Science (2018), 10.1126/science.aat0939.
[19] R. Kubo, J. Phys. Soc. Jap. **12**, 570 (1957).
[20] D. A. Greenwood, Proc. Phys. Soc. **71**, 585 (1958).
[21] D. J. Evans and G. P. Morriss, *Statistical Mechanics of Nonequilbrium Liquids* (ANU Press, 2013).
[22] E. Runge and E. K. U. Gross, Phys. Rev. Lett. **52**, 997 (1984).
[23] L. Landau and E. Lifshitz, in *Electrodynamics of Continuous Media* (Elsevier, 1984) pp. 86–104.
[24] P. Allen, in *Conceptual Foundations of Materials - A Standard Model for Ground- and Excited-State Properties* (Elsevier BV, 2006) pp. 165–218.
[25] K. Yabana and G. F. Bertsch, Phys. Rev. B **54**, 4484 (1996).
[26] Here we assume that the conductivity is a scalar, as the systems we are interested in this work are isotropic on average. For a more general case where the conductivity is a tensor, three different simulations are required, with $\mathbf{E_0}$ pointing in different directions.
[27] G. F. Bertsch, J.-I. Iwata, A. Rubio, and K. Yabana, Phys. Rev. B **62**, 7998 (2000).
[28] L. Kleinman and D. M. Bylander, Physical Review Letters **48**, 1425 (1982).
[29] H. Childs, E. Brugger, B. Whitlock, J. Meredith, S. Ahern, D. Pugmire, K. Biagas, M. Miller, C. Harrison, G. H. Weber, H. Krishnan, T. Fogal, A. Sanderson, C. Garth, E. W. Bethel, D. Camp, O. Rübel, M. Durant, J. M.

Favre, and P. Navrátil (2012) pp. 357–372.
[30] C. Kittel, *Introduction to Solid State Physics* (Wiley, 2004).
[31] A. Castro, H. Appel, M. Oliveira, C. A. Rozzi, X. Andrade, F. Lorenzen, M. A. L. Marques, E. K. U. Gross, and A. Rubio, Phys. Status Solidi B **243**, 2465 (2006).
[32] X. Andrade, D. Strubbe, U. D. Giovannini, A. H. Larsen, M. J. T. Oliveira, J. Alberdi-Rodriguez, A. Varas, I. Theophilou, N. Helbig, M. J. Verstraete, L. Stella, F. Nogueira, A. Aspuru-Guzik, A. Castro, M. A. L. Marques, and A. Rubio, Phys. Chem. Chem. Phys. **17**, 31371 (2015).
[33] G. Kresse and J. Furthmüller, Physical Review B **54**, 11169 (1996).
[34] N. Ashcroft and L. J. Guild, Phys. Lett. **14**, 23 (1965).
[35] P. L. Silvestrelli, Phys. Rev. B **60**, 16382 (1999).
[36] M. P. Desjarlais, J. D. Kress, and L. A. Collins, Phys. Rev. E **66**, 025401(R) (2002).
[37] V. Recoules and J.-P. Crocombette, Phys. Rev. B **72**, 104202 (2005).
[38] V. Vlček, N. de Koker, and G. Steinle-Neumann, Phys. Rev. B **85** (2012), 10.1103/physrevb.85.184201.
[39] V. U. Nazarov, G. Vignale, and Y.-C. Chang, Physical Review B **89** (2014), 10.1103/physrevb.89.241108.
[40] M. P. Desjarlais, C. R. Scullard, L. X. Benedict, H. D. Whitley, and R. Redmer, Physical Review E **95** (2017), 10.1103/physreve.95.033203.
[41] J. Lindhard, *On the properties of a gas of charged particles* (I kommission hos Munksgaard, 1954).
[42] A. Schleife, Y. Kanai, and A. A. Correa, Phys. Rev. B **91**, 014306 (2015).
[43] M. Born, Zeitschrift für Physik **38**, 803 (1926).
[44] D. V. Sivukhin, Reviews of Plasma Physics **4**, 93 (1966).
[45] P. Echenique, F. G. de Abajo, V. Ponce, and M. Uranga, Nuclear Instruments and Methods in Physics Research Section B: Beam Interactions with Materials and Atoms **96**, 583 (1995).
[46] W. Barletta, J. Bisognano, J. Corlett, P. Emma, Z. Huang, K.-J. Kim, R. Lindberg, J. Murphy, G. Neil, D. Nguyen, C. Pellegrini, R. Rimmer, F. Sannibale, G. Stupakov, R. Walker, and A. Zholents, Nuclear Instruments and Methods in Physics Research Section A: Accelerators Spectrometers, Detectors and Associated Equipment **618**, 69 (2010).
[47] R. Falcone, M. Dunne, H. Chapman, M. Yabashi, and K. Ueda, Journal of Physics B: Atomic, Molecular and Optical Physics **49**, 180201 (2016).
[48] F. F. Chen, in *Introduction to Plasma Physics and Controlled Fusion* (Springer Science + Business Media, 1984) pp. 199–224.
[49] J. Hu, Y. Wang, A. Vallabhaneni, X. Ruan, and Y. P. Chen, Appl. Phys. Lett. **99**, 113101 (2011).
[50] L. Zhu, C. R. Otey, and S. Fan, Appl. Phys. Lett. **100**, 044104 (2012).
[51] X. Zhou and Z. Zhang, J. Appl. Phys. **119**, 175107 (2016).
[52] F. G. Eich, M. D. Ventra, and G. Vignale, Phys. Rev. Lett. **112**, 196401 (2014).
[53] G. Tatara, Phys. Rev. Lett. **114**, 196601 (2015).
[54] F. G. Eich, M. Di Ventra, and G. Vignale, ArXiv e-prints (2016), arXiv:1607.05464 [cond-mat.mes-hall].